Electronic Supplementary Material (ESI) for RSC Advances.

Supplementary Information

Title:

A superrepellent coating with dynamic fluorine chains for frosting suppression: effects of polarity, coalescence and ice nucleation free energy barrier

*Takeo Moriya, Kengo Manabe, Mizuki Tenjimbayashi, Ken Suwabe, Hirotaka Tsuchiya, Takeshi Matsubayashi, Walter Navarrini and Seimei Shiratori**

Center for Material Design Science, School of Integrated Design Engineering, Graduate School of Science and Technology, Keio University, 3-14-1 Hiyoshi, Kohoku-ku, Yokohama, Kanagawa 223-8522 Japan

*Corresponding author: Seimei Shiratori, shiratori@appi.keio.ac.jp

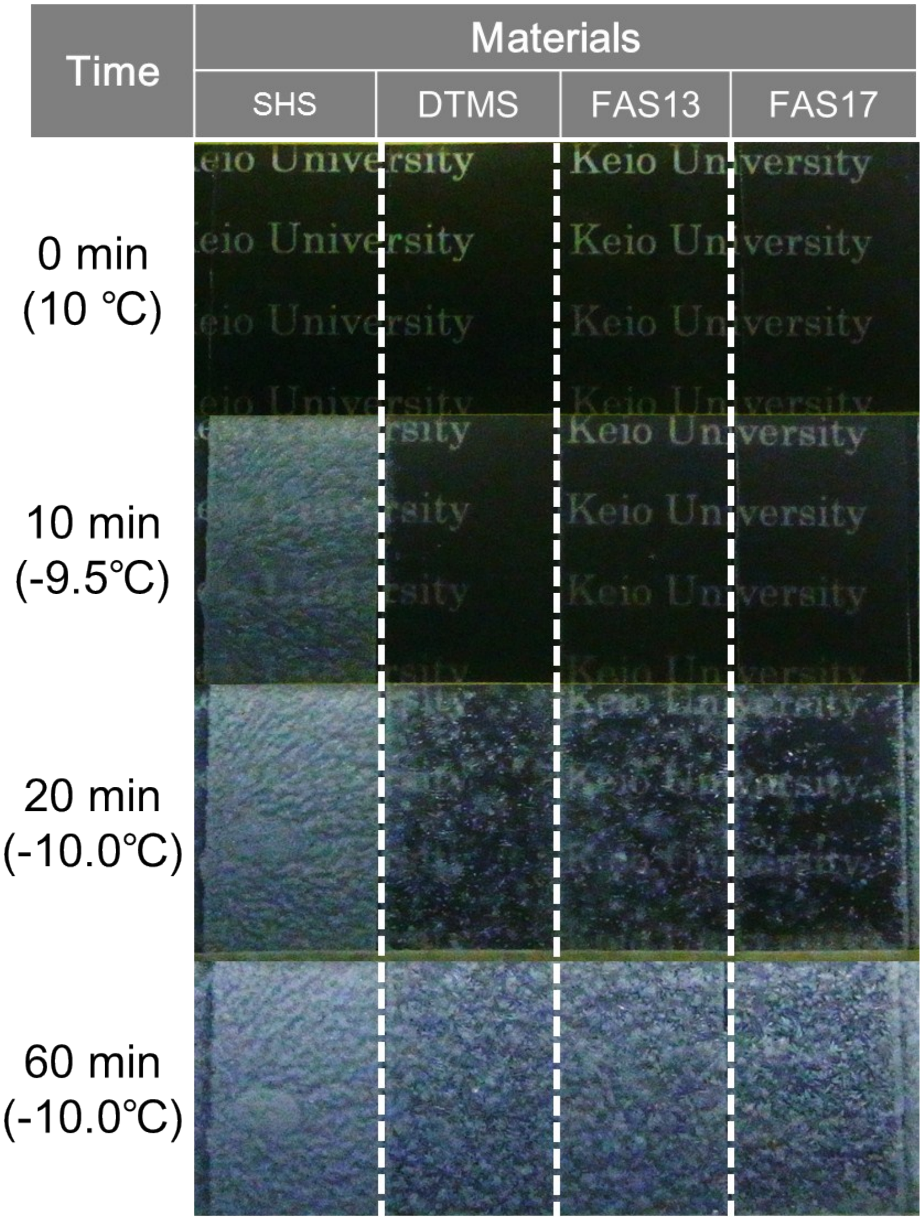

Figure S1. The time-elapsed photographic images during frosting test. Comparison of anti-frosting performance on the coating surface. Superhydrophobic surface (SHS) freezes rapidly compared with other coating surface.

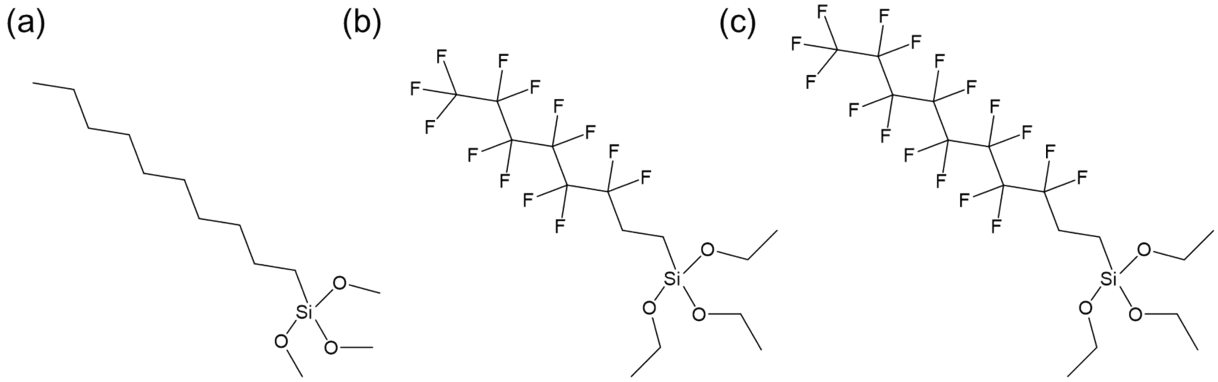

Figure S2. Chemical structures of (a) Decyltrimethoxysilane (DTMS), (b) Tridecafluoro-1,1,2,2-Tetrahydrooctyl-Triethoxy-Silane (FAS13), and (c) Heptadecafluoro-1,1,2,2-Tetrahydrodecyl-Triethoxy-Silane (FAS17)

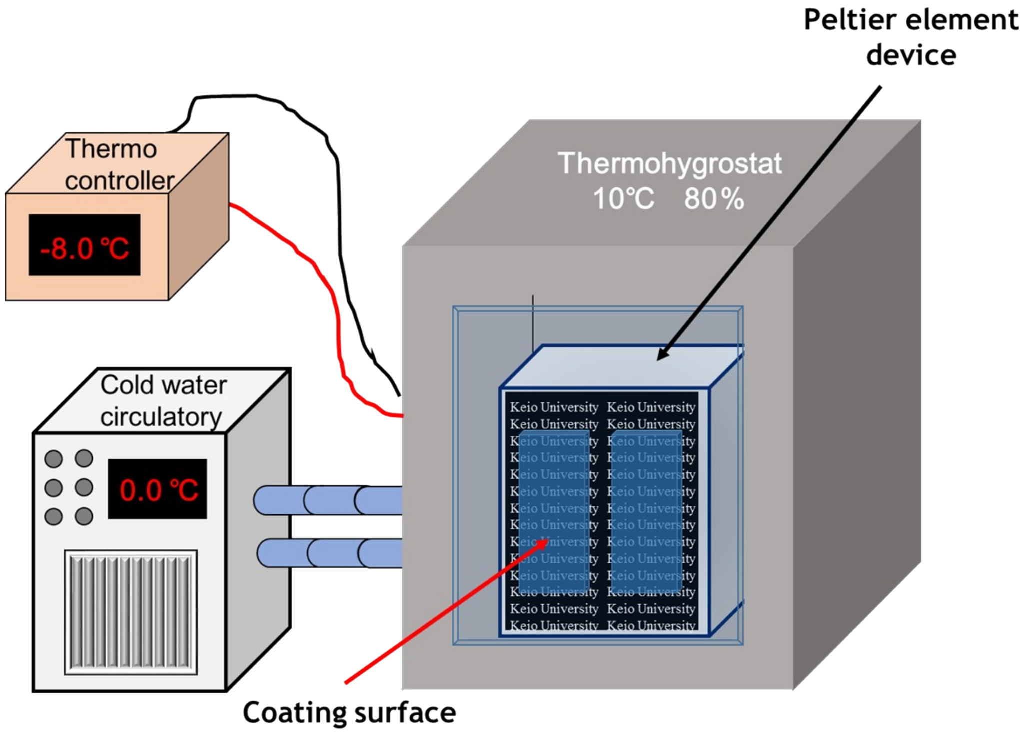

Figure S3. Schematic image of measuring equipment for frosting test.

Field emission scanning electron microscope (FE-SEM) images were taken using a FE-SEM (S-4700, Hitachi, Tokyo, Japan) with an accelerating voltage of 5 kV to characterize the surface nano-topography of the films. FE-SEM images of the coating surface shown in Figure S4 support the proof of smooth surface which could not be observed by FE-SEM.

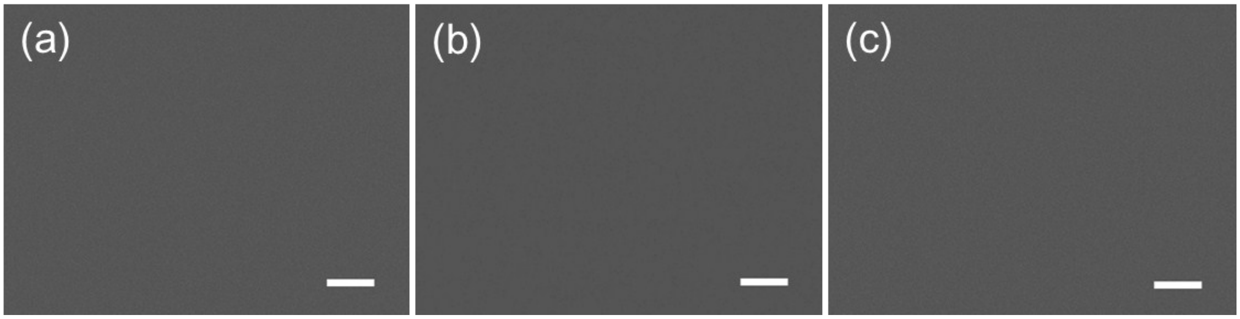

Figure S4. FE-SEM images of the coating surface modified by (a) DTMS, (b) FAS13, (c) FAS17. The white bar size is 200 nm.

The chemical bonds within the coated surface modified by DTMS, FAS13, FAS17 on plasma-treated silicon substrates were examined by Fourier transform infrared spectroscopy (FT-IR) (ALPHA-T, Bruker, Billerica, MA, USA), as shown in Figure S5.

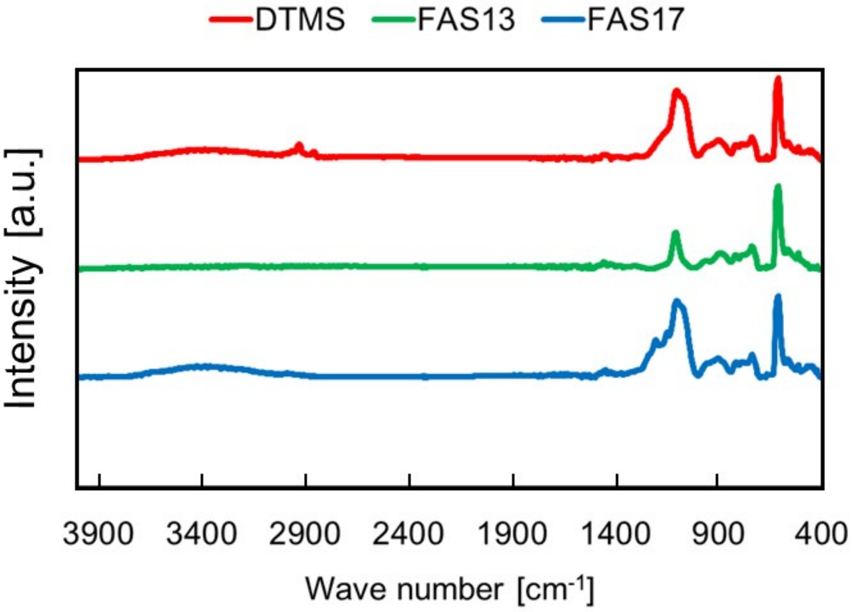

Figure S5. FT-IR spectra of the coating surface modified by DTMS, FAS13, FAS17.

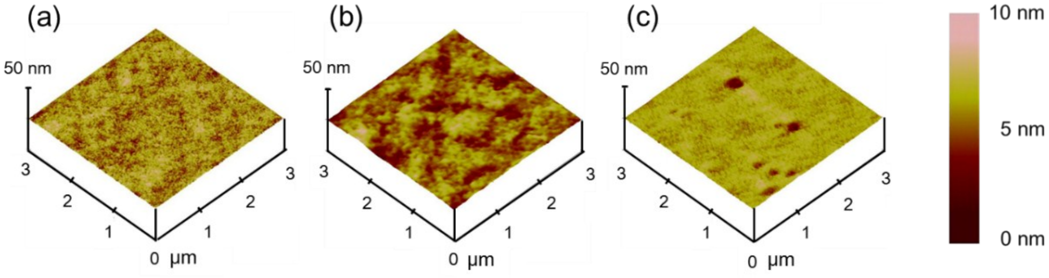

Figure S6. AFM images of glass surfaces coated with (a) DTMS, (b) FAS13, and (c) FAS17. The scan size (x and y) is 3 μm and the data scale (z) is 50 nm.

Film thickness distribution in macro-scale is shown in Figure S7. The coating surface were coated on glass substrate uniformly.

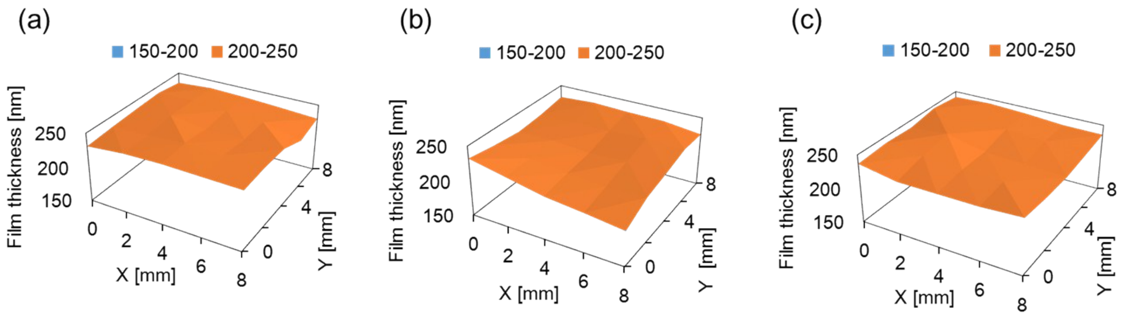

Figure S7. Film thickness distribution of the coating surface modified by (a) DTMS, (b) FAS13, (c) FAS17 were measured by ellipsometry analysis

Table S1. The surface elemental abundance of the three types of coating surface.

Surface elements (atom %)				
Coating surface	C	O	Si	F
DTMS	38.12	40.98	20.90	-
FAS13	17.67	35.55	18.86	27.92
FAS17	14.34	32.66	17.56	35.44

Transmittance in the spectral range from 300 to 1000 nm was measured by a spectrophotometer (UVmini-1240, Shimadzu, Kyoto, Japan).

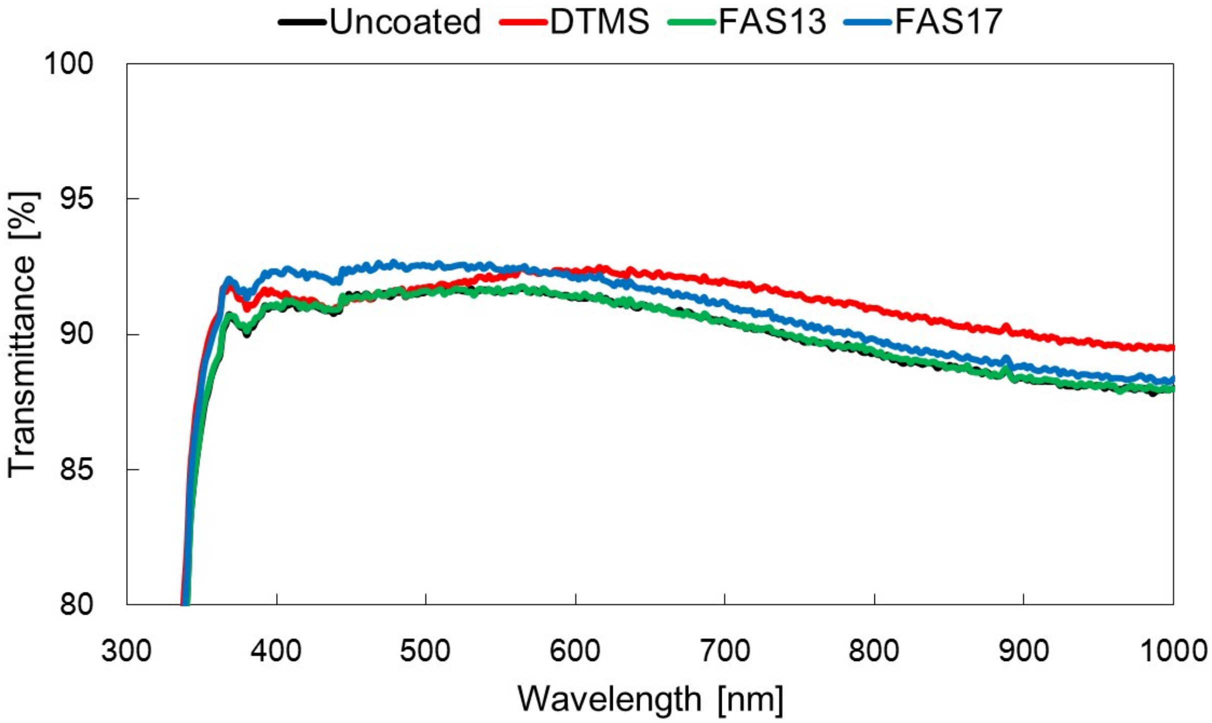

Figure S8. Transmittance of the coating surface modified by DTMS (refractive index: 1.42), FAS13 (refractive index: 1.35), FAS17 (refractive index: 1.33 by spectrophotometer.

Total transmittance (T.T.), parallel transmittance (P.T.), diffusion (DIF) and haze values (HAZE) measurement were carried out using a haze meter (NDH-5000, Nippon Denshoku Industries, Japan) with a white light-emitting diode (5 V, 3 W) as an optical source (Figure S5)

The HAZE, which describes the amount of light scattering when the light passes through the films was calculated by dividing T.T and P.T. by DIF. Haze can be expressed by the following equation:

$$HAZE = \frac{DIF}{T.T} \times 100\ [\%]$$

where $HAZE$, DIF and $T.T.$ are the optical values of haze, diffusion and total transmittance, respectively.

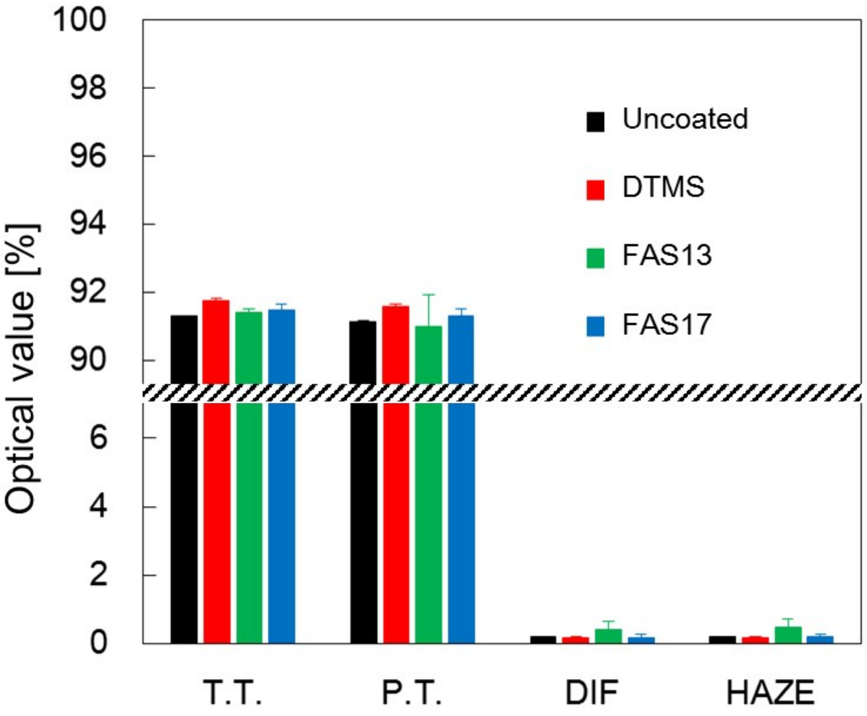

Figure S9. Total transmittance (T.T.), parallel transmittance (P.T.), diffusion (DIF) and haze (HAZE) of the glass substrate and the coating surface modified by DTMS, FAS13, FAS17.

The solid surface energy was calculated with simultaneous equations which the polarity factors of water, formamide and hexadecane (Table S1) and contact angle of each liquid were substituted for equation (1).

Table S2. The polarity factors of water, formamide, hexadecane.

Liquid	γ_L [mN/m]	$\gamma_L{}^{LW}$ [mN/m]	$\gamma_L{}^{+}$ [mN/m]	$\gamma_L{}^{-}$ [mN/m]
Water	72.8	21.8	25.5	25.5
Formamide	58.0	39.0	2.28	39.6
Hexadecane	27.6	27.6	0	0

The polarity factors of solid surface were calculated by equation (1) – (3) (Table S2). .

Table S3. The polarity factors of the coating surface modified by DTMS, FAS13, FAS17.

Material	$\sqrt{\gamma_s{}^{LW}}$ [$\sqrt{mN/m}$]	$\sqrt{\gamma_s{}^{+}}$ [$\sqrt{mN/m}$]	$\sqrt{\gamma_s{}^{-}}$ [$\sqrt{mN/m}$]	$\gamma_s{}^{AB}$ [mN/m]	γ_s[mN/m]
DTMS	4.88	1.07	0.02	0.05	23.86
FAS13	3.87	0.33	1.48	0.98	15.95
FAS17	3.78	0.46	0.87	0.81	15.08

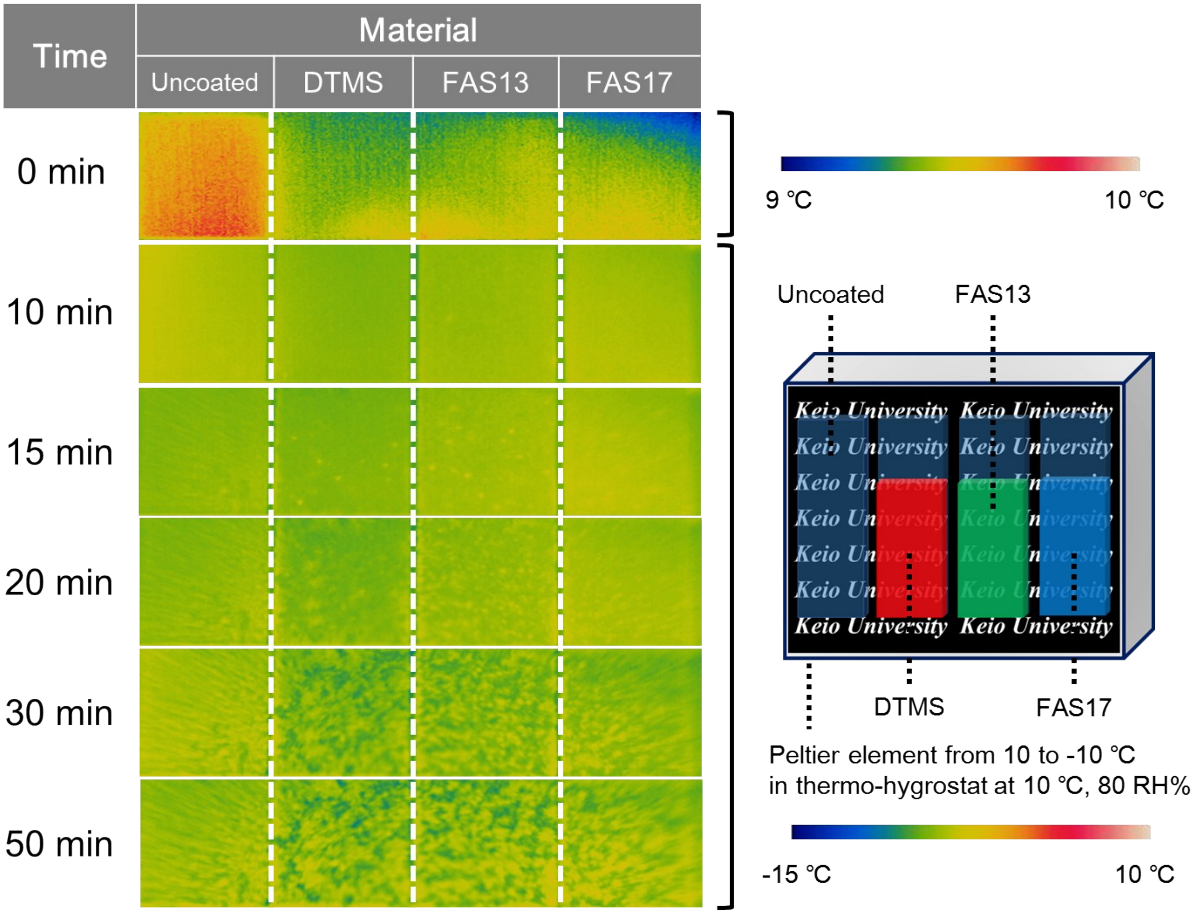

Figure S10. Thermographic images captured during the frosting test to measure surface temperature. These figures showed surface temperature on sample surface. These surface temperatures were almost same.

After 60 minutes from frosting test starts, the unit was heated to 10 ℃ to compare frost removal ability as shown in Figure S11.

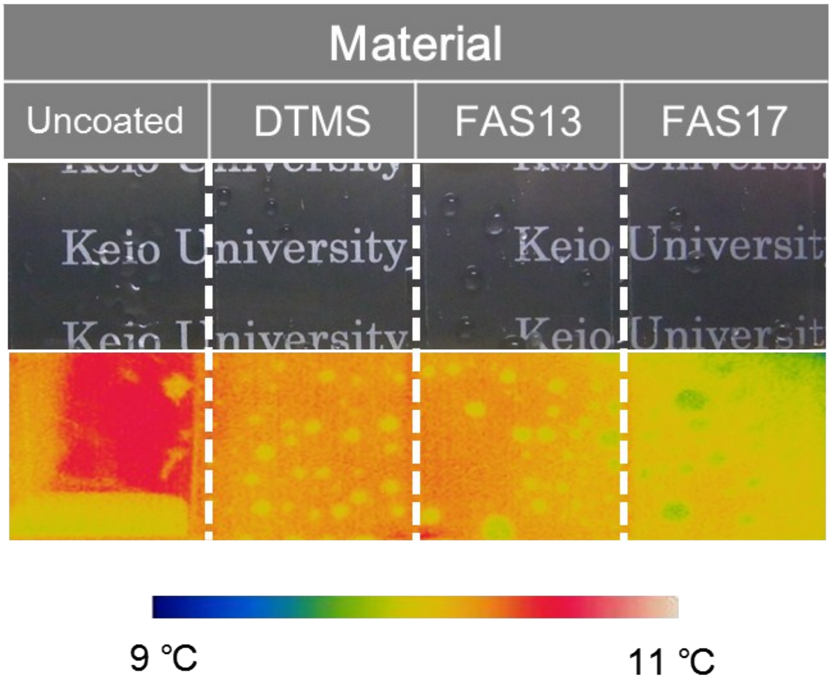

Figure S11. Photographic images and thermography images of heating sample after frosting test.

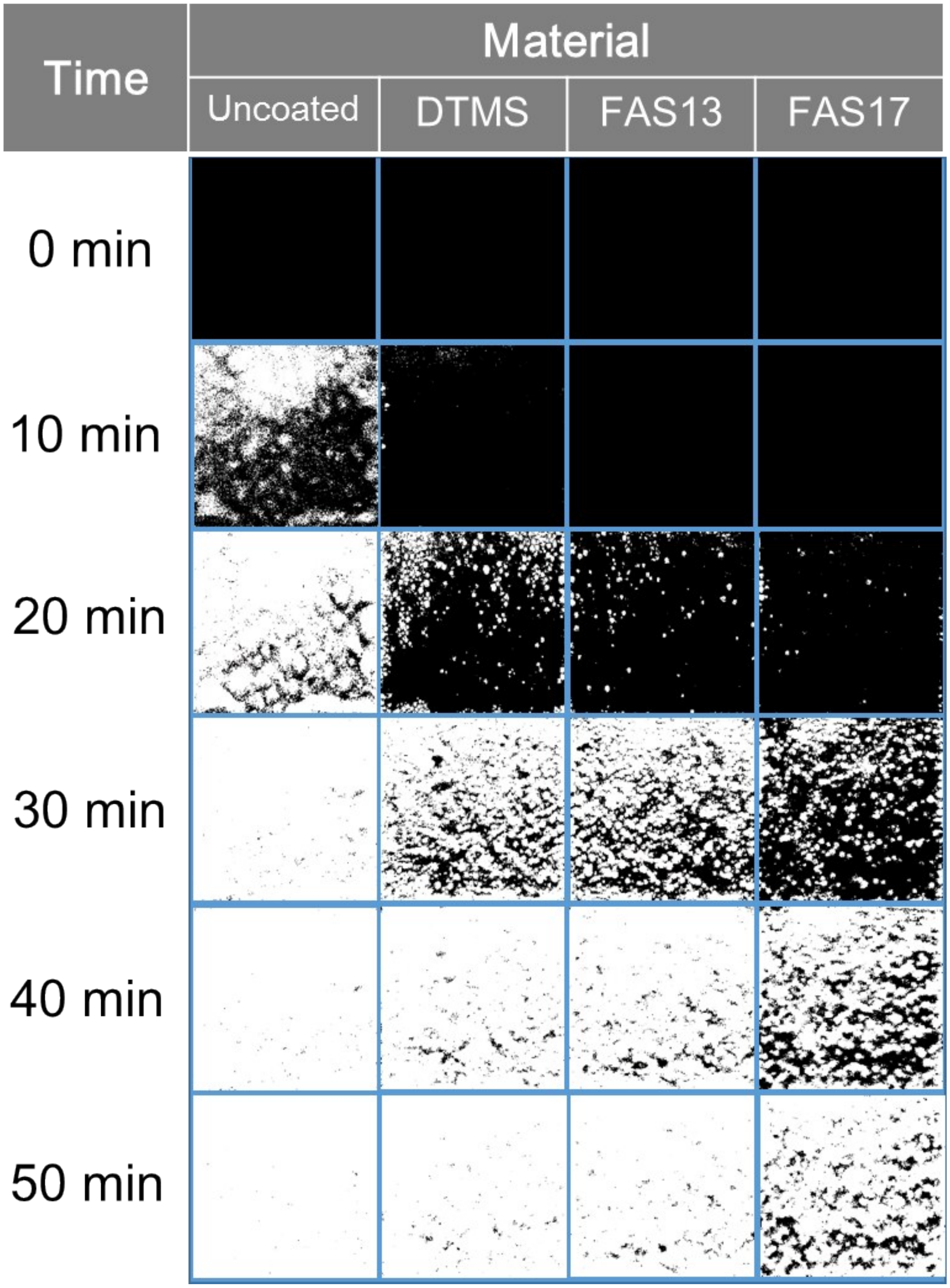

Figure S12. The binarized photographic images during frosting test at interval of five minutes to calculate ice area ratio.

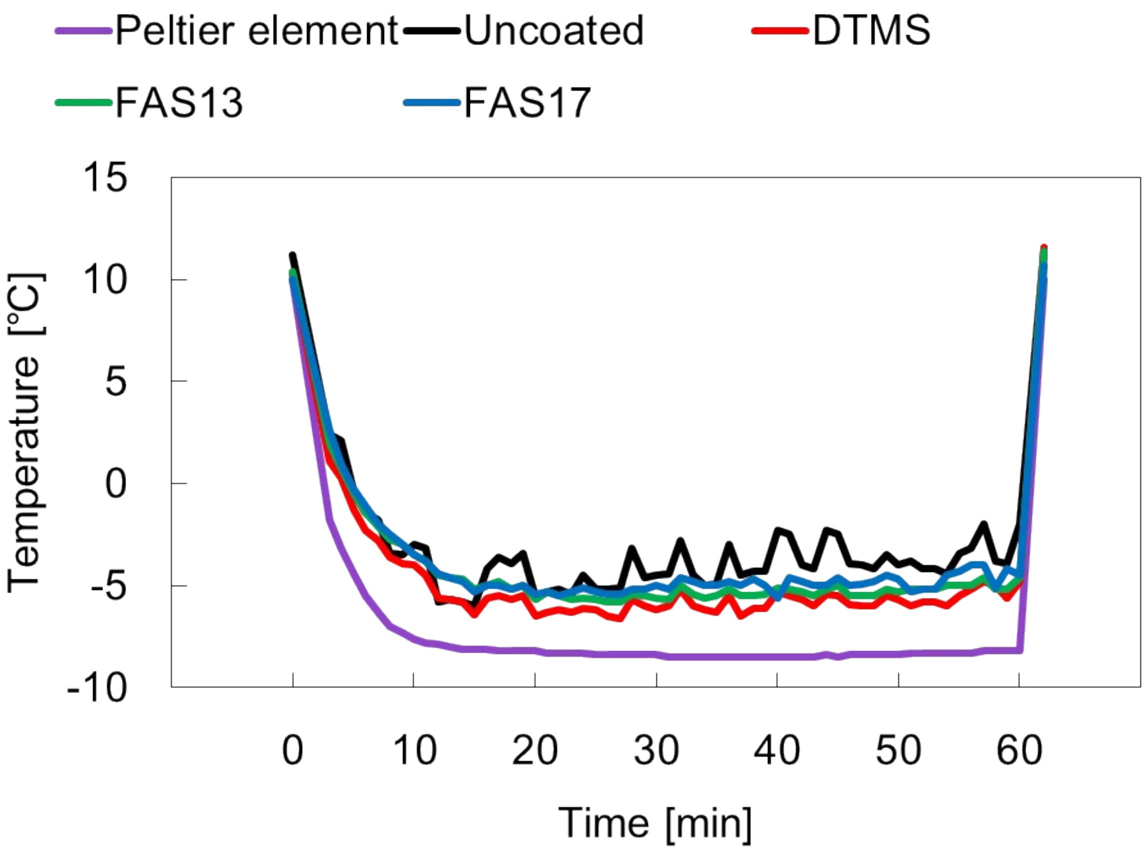

Figure S13. The surface temperature with the glass substrate and the coating surface modified by DTMS, FAS13, FAS17 versus time.

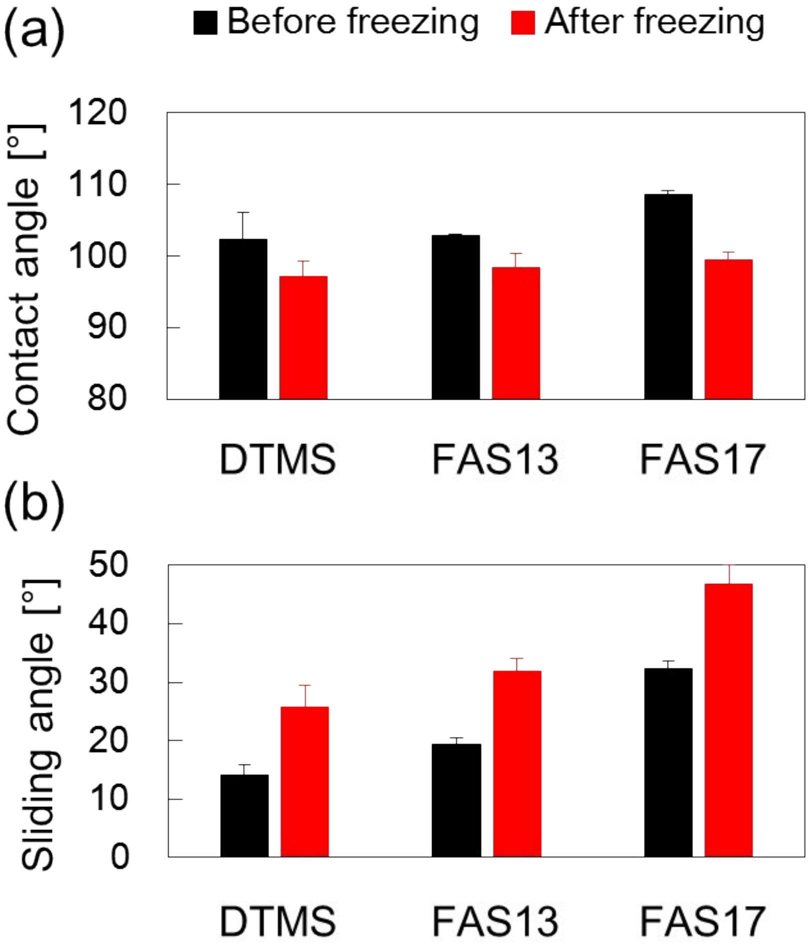

Figure S14. Comparison of (a) water contact angles and (b) sliding angles of water on the surfaces coated by DTMS, FAS13 and FAS17 before freezing with after freezing.

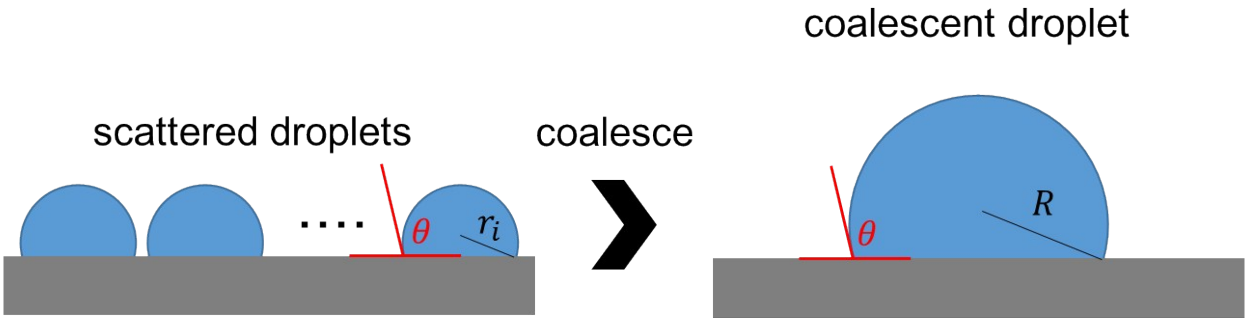

Figure S15. Schematic images of the scattered droplets and coalescent droplet. r_i: the scattered water droplet radius of curvature, R: the coalescent water droplet radius of curvature, θ: contact angle of water droplet on solid surface.

v_i: the volume of one of the scattered droplet

$$v_i = \int_0^\theta \pi (r_i \sin\theta)^2 r_i \sin\theta d\theta = \pi {r_i}^3 \int_0^\theta \sin^3\theta \, d\theta = \pi {r_i}^3 \frac{(1-\cos\theta)^2(2+\cos\theta)}{3} \tag{S1}$$

V: the volume of coalescent droplet

$$V = \int_0^\theta \pi (R\sin\theta)^2 R\sin\theta d\theta = \pi R^3 \frac{(1-\cos\theta)^2(2+\cos\theta)}{3} \tag{S2}$$

Since, the volume of the scattered droplets and the coalescent droplet is the same.

$$v_1 + v_2 + \ldots + v_n = \sum_i^n v_i = V \tag{S3}$$

$$\sum_i^n \pi {r_i}^3 \frac{(1-\cos\theta)^2(2+\cos\theta)}{3} = \pi R^3 \frac{(1-\cos\theta)^2(2+\cos\theta)}{3} \tag{S4}$$

$$R = \left(\sum_{i}^{n} {r_i}^3\right)^{\frac{1}{3}} \tag{S5}$$

s_i: the contact area between one of the scattered droplets and substrate
S: the contact area between coalescent droplet and substrate

$$s_1 + s_2 + \ldots + s_n = \sum_{i}^{n} s_i = \sum_{i}^{n} \pi(r_i \sin\theta)^2 \tag{S6}$$

$$S = \pi(R \sin\theta)^2 = \pi(\sin\theta)^2 \left(\sum_{i}^{n} {r_i}^3\right)^{\frac{2}{3}} \tag{S7}$$

Here, in order to prove that $\sum_{i}^{n} s_i$ is larger than S, we prove the following equation.

$$\sum_{i}^{n} {r_i}^2 > \left(\sum_{i}^{n} {r_i}^3\right)^{\frac{2}{3}} \tag{S8}$$

To prove the following equation and to prove the above equation is synonymous.

$$\left(\sum_{i}^{n} {r_i}^2\right)^3 > \left(\sum_{i}^{n} {r_i}^3\right)^2 \tag{S9}$$

<Proof>

$$\left(\sum_{i}^{n} {r_i}^2\right)^3 - \left(\sum_{i}^{n} {r_i}^3\right)^2$$

$$= \left\{\sum_{i}^{n} {r_i}^6 + 3\sum_{i>j} {r_i}^4 {r_j}^2 + 3\sum_{i>j} {r_i}^2 {r_j}^4 + 6\sum_{i>j>k} {r_i}^2 {r_j}^2 {r_k}^2\right\} - \left\{\sum_{i}^{n} {r_i}^6 + 2\sum_{i>j} {r_i}^3 {r_j}^3\right\}$$

$$= 3\sum_{i>j} {r_i}^4 {r_j}^2 + 3\sum_{i>j} {r_i}^2 {r_j}^4 - 2\sum_{i>j} {r_i}^3 {r_j}^3 + 6\sum_{i>j>k} {r_i}^2 {r_j}^2 {r_k}^2$$

$$= \sum_{i>j} r_i^{\,2} r_j^{\,2} \{3(r_i - r_j)^2 + 4 r_i^{\,2} r_j^{\,2}\} + 6 \sum_{i>j>k} r_i^{\,2} r_j^{\,2} r_k^{\,2} > 0$$

$$\therefore \left(\sum_i^n r_i^{\,2}\right)^3 > \left(\sum_i^n r_i^{\,3}\right)^2$$

$$\therefore \sum_i^n s_i > S$$

<Q. E. D>

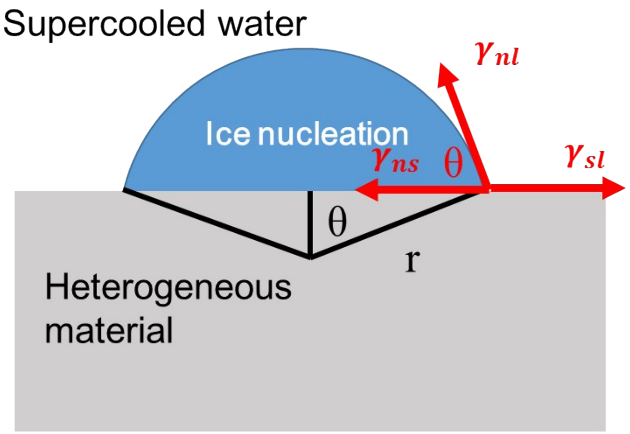

Figure S16. Schematic images of heterogeneous ice nucleation in supercooled water. $\Delta\mu_v$: the Gibb's free energy change per unit volume difference between ice and liquid water, γ_{nl}: interfacial tension between ice nucleation and liquid, r: ice nucleation radius of curvature, θ: contact angle between ice nucleation and solid surface.

(S10) relates with the interfacial tensions between the three interfaces: nucleation-liquid, liquid-solid and solid-liquid.

$$\gamma_{ns} + \gamma_{nl} \cos\theta = \gamma_{sl} \qquad \text{(S10)}$$

S_{nl}: Area of interface between ice nucleation and liquid phase

S_{ns}: Area of interface between ice nucleation and solid phase (heterogeneous material)

$$S_{nl} = \int_0^\theta 2\pi r^2 \sin\theta d\theta = 2\pi r^2 (1 - \cos\theta) \tag{S11}$$

$$S_{ns} = \pi r^2 \sin^2\theta \tag{S12}$$

ΔG_s: total surface energy of heterogeneous nucleation

$$\Delta G_s = 2\pi r^2 \gamma_{nl} (1 - \cos\theta) + \pi r^2 (\gamma_{ns} - \gamma_{sl}) \sin^2\theta \tag{S13}$$

V: volume of ice nucleation

$$V = \int_0^\theta \pi (r \sin\theta)^2 r \sin\theta d\theta = \pi r^3 \int_0^\theta \sin^3\theta \, d\theta = \pi r^3 \frac{(1 - \cos\theta)^2 (2 + \cos\theta)}{3} \tag{S14}$$

ΔG: Free energy change (one ice nucleation) between liquid phase and solid phase

$$\Delta G_{hetero} = - \Delta\mu_v V + \Delta G_s \tag{S15}$$

(S15) is derived by substituting equation of V and ΔG_s for (S6).

$$\Delta G_{hetero} = \left(\frac{-4\pi r^3 \Delta\mu_v}{3} + 4\pi r^2 \gamma_{nl} \right) \frac{(1 - \cos\theta)^2 (2 + \cos\theta)}{4} \tag{S16}$$

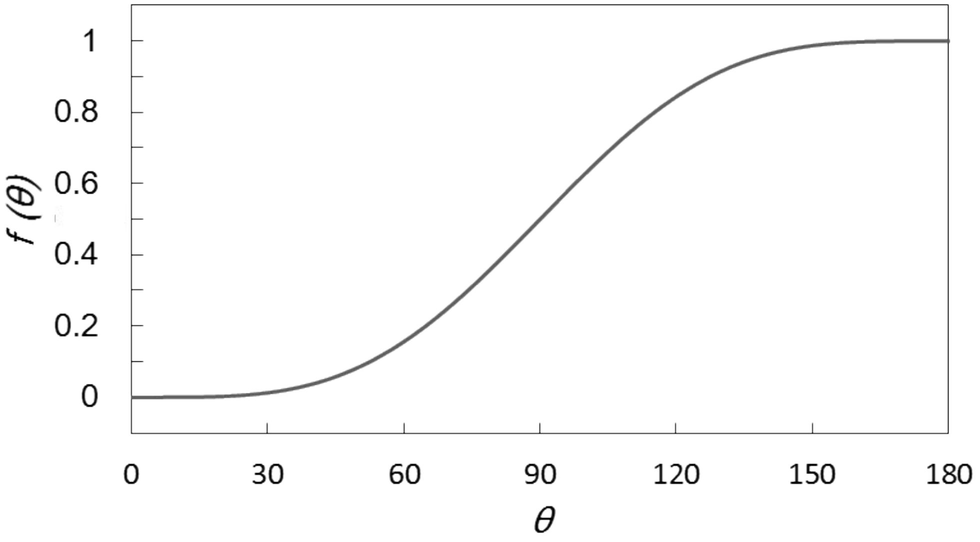

Figure S17. The graph of $f(\theta)$ which is strong factor of the nucleation free energy in the function of θ.

The hückel charge distribution was calculated by extended hückel method with ChemBio3D. In this study, hückel charge of alkyl chain and fluorocarbon were focused. Hückel charge of fluorocarbon was about ten times stronger than that of alkyl chain.

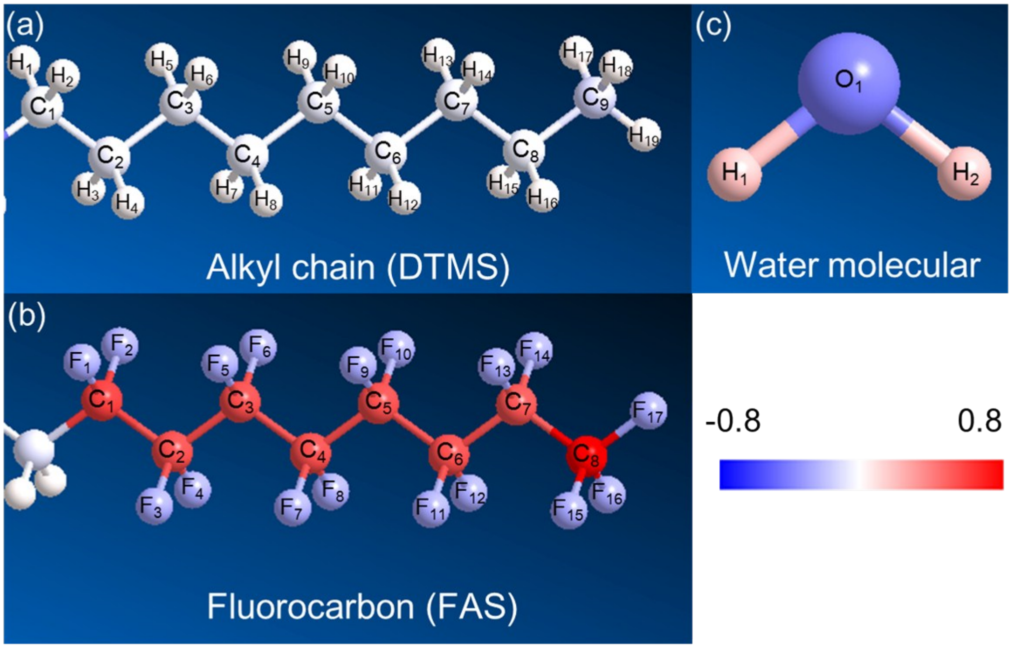

Figure S18. Schematic diagrams of Hückel charge distribution in an (a) alkyl chain, (b) fluorocarbon, and (c) water molecule. Red indicates positive charge and blue indicates negative charge; the color intensity is proportional to the charge strength.

Table S4. Hückel charge distribution of alkyl chain, fluorocarbon and water molecular.

DTMS		FAS		Water molecular	
	Huckel charge		Huckel charge		Huckel charge
C_1	-0.0366417	C_1	0.593714	O_1	-0.405009
C_2	-0.0633116	C_2	0.549497	H_1	0.202504
C_3	-0.055265	C_3	0.551941	H_2	0.202504
C_4	-0.055628	C_4	0.550941		
C_5	-0.0554911	C_5	0.550873		
C_6	-0.0553506	C_6	0.554509		
C_7	-0.0538263	C_7	0.53027		
C_8	-0.0465272	C_8	0.855559		
C_9	-0.128803	F_1	-0.275571		
H_1	0.0255157	F_2	-0.275067		

H_2	0.0255015	F_3	-0.275615		
H_3	0.027733	F_4	-0.27511		
H_4	0.0277485	F_5	-0.275361		
H_5	0.0277607	F_6	-0.275403		
H_6	0.0277456	F_7	-0.275419		
H_7	0.0277603	F_8	-0.275462		
H_8	0.0277755	F_9	-0.275432		
H_9	0.0277835	F_{10}	-0.275475		
H_{10}	0.0277683	F_{11}	-0.275412		
H_{11}	0.0277903	F_{12}	-0.275455		
H_{12}	0.0278055	F_{13}	-0.274427		
H_{13}	0.0279176	F_{14}	-0.27447		
H_{14}	0.0279025	F_{15}	-0.280099		
H_{15}	0.0288415	F_{16}	-0.280151		
H_{16}	0.0288566	F_{17}	-0.280357		
H_{17}	0.038707				
H_{18}	0.0378779				

H_{19}	0.0387221				

We calculated hückel charge by extended hückel charge using ChemBio3D.

φ_i: molecular orbital

χ_r: Normalized valence atomic orbital

$$\varphi_i = \sum_{r=1}^{n} c_{ir}\chi_r \tag{S17}$$

$\hat{H}$: Hamiltonian

H_{rr}: Coulomb integration of valence atomic orbital

H_{rs}: Exchange integration of valence atomic orbital

$$H_{rr} = \int \chi_r \hat{H} \chi_r d\tau \tag{S18}$$

$$H_{rs} = \int \chi_r \hat{H} \chi_s d\tau \ \ (r \neq s) \tag{S19}$$

It is derived secular equation by variational calculus.

S_{rs}: Coulomb integration of valence atomic orbital

$$|H_{rs} - ES_{rs}| = 0 \tag{S20}$$

In extended huckel method, H_{rr}, H_{rs}, are expressed as following equation.

I_r: Ionization potential energy

$$H_{rr} =- I_r \tag{S21}$$

$$H_{rs} = \frac{1.75 \cdot S_{rs}(H_{rr} + H_{rs})}{2} \tag{S22}$$

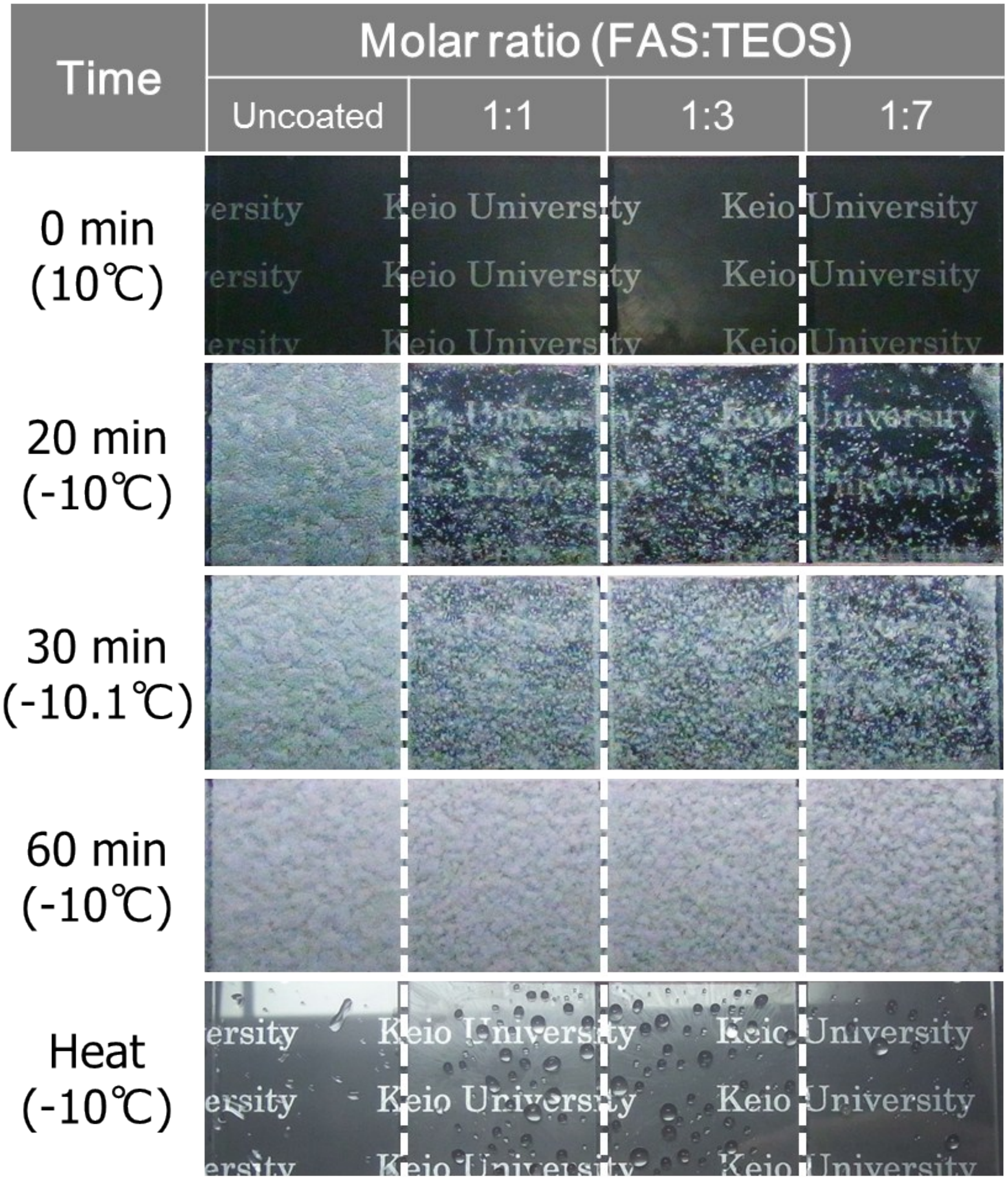

Figure S19. The time-elapsed photographic images of coated surfaces during frosting test. These coated surfaces were fabricated by solutions of different molar ratio FAS and TEOS. We observed that the number of water droplets on the coated surface which was fabricated by the solution whose molar ratio of FAS : TEOS = 1:7 was smaller than those on other surfaces.

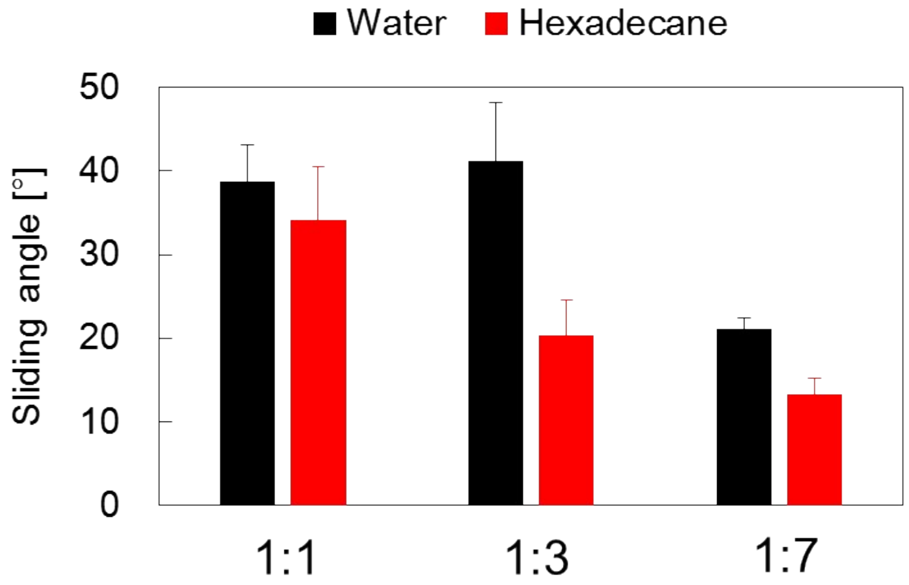

Figure S20. Comparison of sliding angles on the coating surface which change molar ratio FAS to TEOS of the solution.

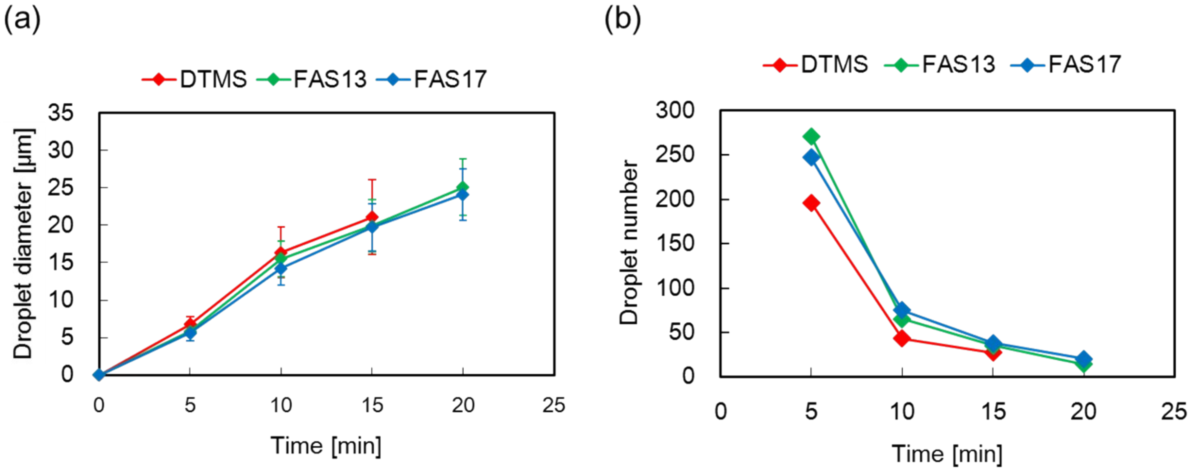

Figure S21. Time dependence of (a) the condensed droplet diameter and (b) the number of condensed droplets on three types of coating surfaces during frosting test.

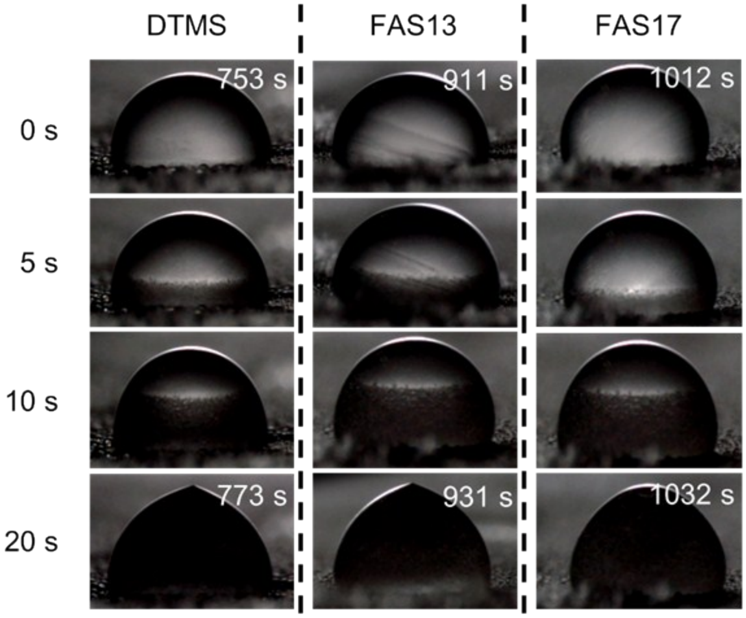

Figure S22. The photographic images of the water droplet which gradually freeze on coating surface. Peltier element in air with a relative humidity of about 40% and temperature of 26.3 °C. A water droplet put on peltier element set at −8±1 °C for 20 min. The droplet volume is 5 μL.